

Article

# Harnessing Greenhouse Gases Absorption by Doped Fullerenes with Externally Oriented Electric Field

Rodrigo A. Lemos Silva <sup>1,\*</sup> , Daniel F. Scalabrini Machado <sup>2</sup> , Núbia Maria Nunes Rodrigues <sup>3</sup>,  
Heibbe C. B. de Oliveira <sup>4</sup> , Luciano Ribeiro <sup>3</sup> and Demétrio A. da Silva Filho <sup>1,\*</sup> 

<sup>1</sup> Institute of Physics, University of Brasília, Brasília 70919-970, Brazil

<sup>2</sup> Laboratório de Modelagem de Sistemas Complexos (LMSC), Instituto de Química, Universidade de Brasília, Brasília 70919-970, Brazil; daniel.scalabrini@unb.br

<sup>3</sup> Grupo de Química Teórica e Estrutural de Anápolis, Campus de Ciências Exatas de Anápolis, Universidade Estadual de Goiás, Anápolis 75132-903, Brazil; nubiamarianunes@gmail.com (N.M.N.R.); lribeiro@ueg.br (L.R.)

<sup>4</sup> Laboratório de Estrutura Eletrônica e Dinâmica Molecular (LEEDMOL), Instituto de Química, Universidade Federal de Goiás, Goiânia 74001-970, Brazil; heibbe@ufg.br

\* Correspondence: silvarodrigo021@gmail.com (R.A.L.S.); dasf@unb.br (D.A.d.S.F.)

**Abstract:** In this work, a theoretical investigation of the effects caused by the doping of C<sub>20</sub> with silicon (Si) atom as well as the adsorption of CO, CO<sub>2</sub> and N<sub>2</sub> gases to C<sub>20</sub> and C<sub>19</sub>Si fullerenes was carried out. In concordance with previous studies, it was found that the choice of the doping site can control the structural, electronic, and energetic characteristics of the C<sub>19</sub>Si system. The ability of C<sub>20</sub> and C<sub>19</sub>Si to adsorb CO, CO<sub>2</sub> and N<sub>2</sub> gas molecules was evaluated. In order to modulate the process of adsorption of these chemical species to C<sub>19</sub>Si, an externally oriented electric field was included in the theoretical calculations. It was observed that C<sub>19</sub>Si is highly selective with respect to CO adsorption. Upon the increase of the electric field intensity the adsorption energy was magnified correspondingly and that the interaction between CO and C<sub>19</sub>Si changes in nature from a physical adsorption to a partial covalent character interaction.

**Keywords:** C<sub>20</sub> fullerene; C<sub>19</sub>Si; doping; external electric field; carbon monoxide; sensor



**Citation:** Lemos Silva, R.A.; Scalabrini Machado, D.F.; Nunes Rodrigues, N.M.; de Oliveira, H.C.B.; Ribeiro, L.; da Silva Filho, D.A. Harnessing Greenhouse Gases Absorption by Doped Fullerenes with Externally Oriented Electric Field. *Molecules* **2022**, *27*, 2968. <https://doi.org/10.3390/molecules27092968>

Academic Editor: Yan'an Gao

Received: 1 March 2022

Accepted: 29 April 2022

Published: 6 May 2022

**Publisher's Note:** MDPI stays neutral with regard to jurisdictional claims in published maps and institutional affiliations.



**Copyright:** © 2022 by the authors. Licensee MDPI, Basel, Switzerland. This article is an open access article distributed under the terms and conditions of the Creative Commons Attribution (CC BY) license (<https://creativecommons.org/licenses/by/4.0/>).

## 1. Introduction

Carbon nanostructures have been continuously studied for the most diverse applications [1–6]. Among these nanostructures, fullerenes [7,8] stand out because of their good physicochemical reactivity and their symmetrical and relatively simple structure [9,10]. These characteristics render fullerenes, whether in their pristine or doped form, an attractive molecular system to be object of several theoretical studies aiming at various sorts of applications [11–16].

Among the fullerenes, C<sub>20</sub> is the smallest known example containing only twelve pentagonal faces. Since the existence of this allotrope of carbon was already predicted [17], even before its experimental discovery [18], C<sub>20</sub> and its derivatives already had an extensive history of studies [19–22].

Considered the most reactive of the fullerenes [18], interest in C<sub>20</sub> has continued over time [23–27]. This molecule has been the object of several studies that aim to carry out its doping to investigate aspects related to its electronic and structural characteristics, in addition to proposing possible applications in different areas.

In a recent theoretical investigation, Metin and co-authors [15] used calculations with the theoretical chemistry model B3LYP/6-31G(d) to investigate both the hydrogen storage capacity and the electronic properties of C<sub>20</sub>, C<sub>15</sub>M<sub>5</sub> and H<sub>2</sub>@C<sub>15</sub>M<sub>5</sub>, with M = Al, Si, Ga, Ge. Among the conclusions of the research, the authors highlighted that, fullerenes doped with Si and Ge, more specifically in the form C<sub>15</sub>Si<sub>5</sub> and C<sub>15</sub>Ge<sub>5</sub>, were highly sensitive to the

presence of H<sub>2</sub>. In addition, the ability of C<sub>20</sub>-doping to manipulate the physicochemical and structural parameters of fullerenes was also confirmed.

The analysis of C<sub>20</sub>, in its pure form and doped with aluminum (C<sub>20-n</sub>Al<sub>n</sub>;  $n = 1-5$ ), was recently performed by Hassanpour and coauthors [23]. In a theoretical effort, employing various levels of Density Functional Theory (DFT) calculations, they investigated the Al substitution in the C<sub>20</sub> cage. Through analysis of the infrared spectrum (Infrared-IR), the authors observed that both the number and the position of Al atoms can change the IR spectrum. Furthermore, they observed that by controlling the number of dopants, the concentration and distribution of atomic charges (APT charges) can be altered to favor adsorption of chemical species to the C<sub>20-n</sub>Al<sub>n</sub> cage.

Amongst the various atoms possible for the doping of C<sub>20</sub>, Si has drawn attention in recent years. The Si atom belongs to the same family as carbon and may have interesting properties when used as an impurity in the cage of carbon nanostructures. Doping of C<sub>20</sub> with Si was theoretically studied by Koochi, Amiri and SHariatl [28], using DFT calculations, the authors analyzed the effects of doping C<sub>20-n</sub>Si<sub>n</sub> with  $n = 1-10$ . This strategy indicates that, in the same vein as in the case of Al doping, controlling the position and number of Si heteroatoms makes it possible to modulate structural changes of the molecule as well as the energies of the molecular orbitals. Similar results were also observed theoretically by Ajeel and co-authors [29].

Beside the aforementioned examples, there are interest in applying C<sub>20</sub> and its derivatives for the most varied purposes, whether for hydrogen storage [15], as a drug delivery system [30,31] or for the detection of biomolecules [32]. A very promising application of these carbonaceous systems is in detection and capture of many gases [14,33] especially those associated with the greenhouse effect and/or harmful to health.

In this spirit, the present work is dedicated to the study of C<sub>20</sub> and C<sub>19</sub>Si for the adsorption of carbon monoxide (CO) and carbon dioxide (CO<sub>2</sub>). Both CO and CO<sub>2</sub> are products of burning fossil fuels. While CO<sub>2</sub> is one of the main gases responsible for the greenhouse effect, along with methane gas, CO contamination is considered by the World Health Organization as one of the main causes of accidental poisoning around the world each year [34].

Theoretical DFT-based calculations were carried out to investigate the effects of the interaction between C<sub>19</sub>Si and CO and CO<sub>2</sub> molecules. Recently, there has been much attention to the use of externally oriented electric fields (EOEF) to harness physical and chemical properties of molecular systems [35–37]. Intermolecular interactions between weakly interacting systems can be strongly aided by EOEFs, since it has the advantage of being easy to achieve and control, and is environmentally friendly [38]. On the realm of molecular sensors, previous works [16,39–43], have demonstrated that the adsorption of molecules and the storage of H<sub>2</sub> can be facilitated in the presence of an EOEF. Additionally, EOEF might render selectivity to the sensor towards a given species in complex gaseous mixtures [16,39].

Based in our interest in theoretical investigations aiming at the development of new sensors [44], we disclose herein the influence of an externally oriented electric field to rationally control the adsorption process of gas molecules on doped C<sub>19</sub>Si fullerenes relying on DFT calculations. Since approximately 78% of the Earth's atmosphere is made up of nitrogen gas (N<sub>2</sub>) [45], the selectivity of C<sub>19</sub>Si for the detection of CO and CO<sub>2</sub> was evaluated by comparing the adsorption energy between the C<sub>19</sub>Si cage and the CO, CO<sub>2</sub> and N<sub>2</sub> molecules.

## 2. Materials and Methods

To confirm the structural and electronic trends observed in the fullerene cage after doping with a silicon atom, an investigation involving several theoretical levels was carried out. In all calculations, unrestricted optimizations were performed. The absence of negative frequencies confirmed that the molecules are at their energetic and structural minimum at each theoretical level considered. Several combinations of Exchange

Correlation DFT functionals and basis sets ( $\omega$ B97XD/6-31G(d),  $\omega$ B97XD/6-311+G(d,p),  $\omega$ B97XD/def2TZVP, M062X/6-31G(d), M062X/6-311+G(d,p), M062X/def2TZVP, M06L/6-31G(d), M06L/6-311G(d,p), M06L/def2TZVP, B3LYP/6-31G(d), B3LYP/6-311+G(d,p) and B3LYP/def2TZVP) were tested to screen electronic and structural properties of pristine and doped fullerenes. The screening of the theoretical model on the electronic and structural properties revealed the following combination of DFT Exchange-correlation function and basis set,  $\omega$ B97XD/6-31G(d) and  $\omega$ B97XD/6-311+G(d,p), as the optimal choice for the investigation of the dimers interaction considering the compromise of accuracy and computation cost. While the 6-31G(d) basis set has been reported to be a good choice for obtaining fairly reliable results in fullerenes [11,46], using the more extended 6-311+G(d,p) basis set improves the description of the non-covalent interactions, for further analysis of Quantum Theory of Atoms in Molecules (QTAIM) parameters and Reduced Density Gradient (RDG) properties as reported in recent studies [47,48].

Adsorption energies under electric field  $F$ , were calculated using the supramolecular approach considering the optimized structures by the expression [49],

$$E_{ads}(F) = E_{gas-C_{19}X}(F) - [E_{gas}(F) + E_{C_{19}X}(F)]; X = Si \text{ or } C. \quad (1)$$

In Equation (1),  $E_{ads}(F)$  is the adsorption energy.  $E_{gas-C_{19}X}(F)$  refers to the energy of the dimer formatted by the  $C_{19}X$  and the gas molecules,  $E_{gas}(F)$  is the energy of the gas molecule and  $E_{C_{19}X}(F)$  is the energy of the fullerene  $C_{20}$ , for  $X = C$  or  $C_{19}Si$  for  $X = Si$ .

The adsorption energies were corrected for the Basis Set Superposition Error (BSSE) using the Counterpoise method [50]. The calculations included EOE,  $F$ , in atomic units (a.u.) (1 a.u. = 51 V/Å) in the range:  $F = 0.000$  a.u., 0.001 a.u., 0.005 a.u., 0.010 a.u., 0.020 a.u. and 0.025 a.u. along the Si heteroatom (see Figure S1 for clarity).

The description of intermolecular interactions was performed by means of the QTAIM [51–53] and RDG analysis [54,55]. Molecular Electrostatic Potential (MEP) map, electronic and structural properties were calculate with the Gaussian 16 [56] software. QTAIM and RDG properties were calculated using Multiwfn [57] wave function analysis program. VMD software version 1.9.3 [58] was employed to render isosurfaces and molecular representations.

### 3. Results and Discussion

#### 3.1. Doping Effects on the Electronic and Structural Properties of Fullerenes

The structure of doped fullerene was constructed by replacing a carbon atom for a silicon atom. Initially, the molecules had their structures optimized at the  $\omega$ B97XD/6-31G(d) level of theory followed by another round of calculation at the  $\omega$ B97XD/6-311+G(d,p) model chemistry. Both pure and doped fullerene are shown in Figure 1 and the respective coordinates of these molecules are shown in the Supplementary Materials (SM) Table S1.

From Figure 1 we clearly note that Si-doping promoted remarkable structural deformations of the fullerene cage. Due to its larger atomic radius, it was observed that the Si-C bond distances with the adjacent C-atoms was lengthened with respect to the C-C bond distances prior to the substitution. From a polarization perspective, Merz-Kollman (MK) charge analysis (using the 6-31G(d) basis set and in parenthesis with 6-311+G(d,p)) indicates that  $C_{20}$  has a modest charge distribution ranging from  $-0.018$  ( $-0.103$ ) to  $0.018$  ( $0.103$ )e (Figure 1D). For the  $C_{19}Si$ , MK charges range from  $-0.341$  ( $-0.366$ ) to  $0.341$  ( $0.366$ )e (Figure 1E). Still on Figure 1D, it was also noted charge accumulation of  $-0.222$  ( $-0.162$ )e on the Si-atom. MEPs shown in Figure 1D,E shows that, Si-doping imparts a polarization of the fullerene, with a dipole moment of  $C_{19}Si$  of  $\mu = 1.950$  D (1.460 D) similar to what is observed in reported studies in literature [25,29]. As an immediate result of the polarization of the molecule, the effective intermolecular interaction can be strongly altered [11,59–61], so that  $C_{19}Si$  display the ability to adsorb different molecular species aided by electrostatic forces (dipole-dipole, for instance) that was once absent in its pristine form.

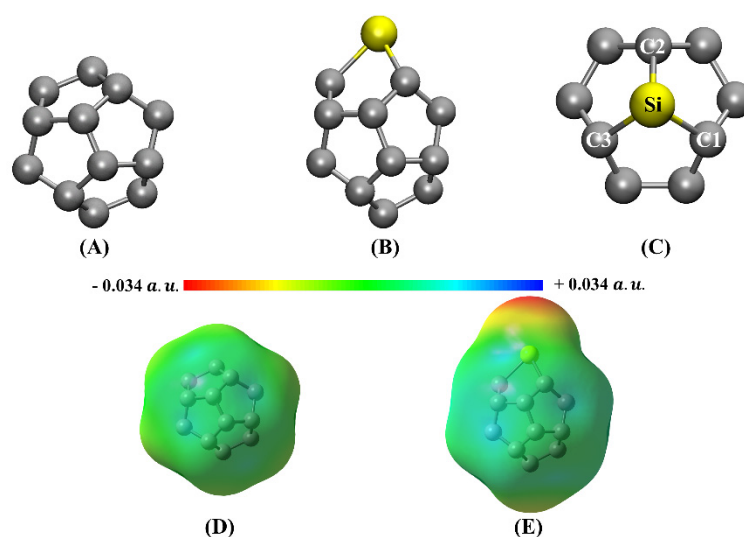


**Figure 1.** Optimized geometries of the (A)  $C_{20}$  and (B)  $C_{19}Si$  fullerenes as obtained at the  $\omega B97XD/6-311+G(d,p)$  level of theory. (C) brings an upper view perspective of the  $C_{19}Si$  structure. Molecular Electrostatic Potential (MEP) map of (D)  $C_{20}$  and (E)  $C_{19}Si$ .

Doping the  $C_{20}$  fullerene had direct impact on the electronic structure. Looking at the frontier eigenstates (HOMO and LUMO), shown in Table S3, addition of an Si-atom induced an increase in the HOMO-LUMO energy gap,  $E_{HL} \sim 0.3$  eV: for  $C_{20}$  fullerene,  $E_{HL} = 5.46$  eV (6-31G(d)) and,  $E_{HL} = 5.40$  eV (6-311+G(d,p)) whereas for  $C_{19}Si$  DFT calculations delivered  $E_{HL} = 5.81$  eV (6-31G(d)) and  $E_{HL} = 5.72$  eV (6-311+G(d,p)). Thus, it is noted that the increase in  $E_{HL}$  is a trend observed for both bases used. It is important to highlight that, in previous works, the doping of nanocarbon structures, including fullerenes  $C_{60}$  [62,63] and fullerenes  $C_{20}$  [64,65], led to a decrease in the value of  $E_{HL}$ , which differs from the results observed in this work. Additionally, regarding the variation of the energy gap between the frontier orbitals, it is observed that the negative MK charges on the Si atom (see the MEP in Figure 1E), are not in line with the atomic charge on the heteroatom observed in the literature for  $C_{19}Si$  [14,30].

To investigate whether such contradictions is an artifact of the level of theory employed, we performed additional unrestricted optimizations with different Exchange-Correlation DFT functionals (XCF) and basis set (see Materials and Methods section) keeping track to the absence of negative frequencies. The results of such extended theoretical survey on the frontier orbitals, as obtained at the B3LYP/6-31G(d), B3LYP/6-311+G(d,p), B3LYP/def2TZVP,  $\omega B97XD/6-31G(d)$ ,  $\omega B97XD/6-311+G(d,p)$ ,  $\omega B97XD/def2TZVP$ , M06L/6-31G(d), M06L/6-311+G(d,p), M06L/def2TZVP, M062X/6-31G(d), M062X/6-311+G(d,p) and M062X/def2TZVP are reserved in Tables S3 and S4 found in the SM file to avoid proliferation of tables in the main text. Glancing at Tables S3 and S4 we report the percentual increase of HOMO-LUMO energy gap upon Si-doping,  $\Delta E_{HL}$ , and straightforwardly testify that regardless of the XCF/basis set combination, the addition of a Si-atom increases the chemical stability of  $C_{19}Si$  over  $C_{20}$ . Similarly, the apparent opposite findings of this work and those reported in literature [14,30] concerning the charge accumulation on Si-atom was retained for each of the screened XCF/basis set (see Table S4). From Table S4, partial MK charge on Si-atom, evidently is affected by the choice of XCF/basis set, nevertheless, all theoretical calculations consistently delivered a negative charge on Si. We, therefore, believe there is no dispute concerning this issue. Still on Table S4 we note that the different levels of calculations provoke slightly changes on bond lengths supporting our choice for  $\omega B97XD/6-31G(d)$  and  $\omega B97XD/6-311+G(d,p)$  as a reliable theoretical model for further analysis. Moreover, despite these contradictions with the results reported in some previous works, in which  $C_{20}$  was doped with Si [14,27,30], our calculations is in agreement with other similar works [24,25,29].

To further investigate the possible causes of the difference in results observed in these calculations with the results presented in the literature [14,27,30], and inspired by studies with the doping of  $C_{20}$  with Si and Al [23,28,29] we studied the impact of the position of Si-atoms in the fullerene cage. For this purpose, 20 configurations of  $C_{19}Si$  were produced, named  $C_{19}Si(X)$ , where  $X = 1-20$  indicate the label of the carbon atom replaced by a Si-atom, as depicted in Figure 2. All  $C_{19}Si(X)$  were optimized without restrictions at the  $\omega B97XD/6-311+G(d,p)$  level of theory.

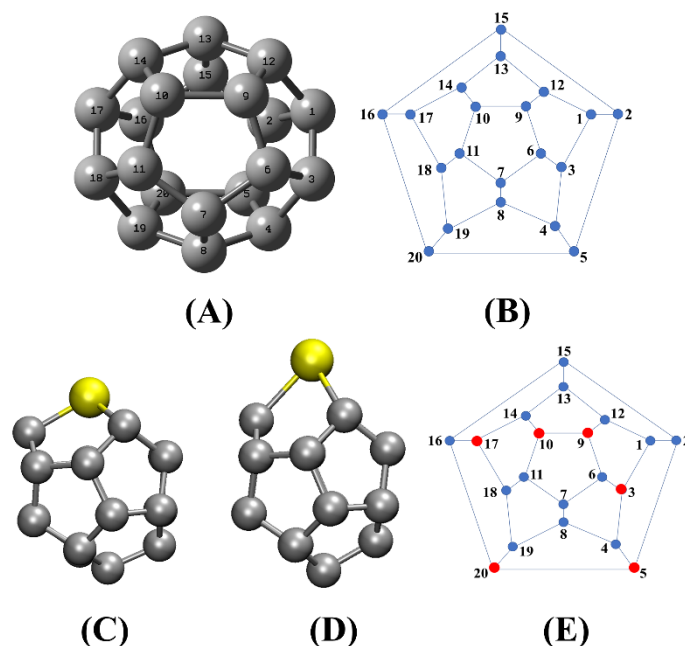


**Figure 2.** (A)  $C_{20}$  fullerene structure and (B) its corresponding Schlegel diagram. The atom indexes are presented to elucidate the Si doping positions. (C) represents the substitutions which produced the set  $C_{19}Si(A)$  formed by:  $C_{19}Si(1)$ ,  $C_{19}Si(2)$ ,  $C_{19}Si(4)$ ,  $C_{19}Si(6)$ ,  $C_{19}Si(7)$ ,  $C_{19}Si(8)$ ,  $C_{19}Si(11)$ ,  $C_{19}Si(12)$ ,  $C_{19}Si(13)$ ,  $C_{19}Si(14)$ ,  $C_{19}Si(15)$ ,  $C_{19}Si(16)$ ,  $C_{19}Si(18)$  and  $C_{19}Si(19)$ . (D) represents the substitutions which produced the set  $C_{19}Si(B)$  formed by:  $C_{19}Si(3)$ ,  $C_{19}Si(5)$ ,  $C_{19}Si(9)$ ,  $C_{19}Si(10)$ ,  $C_{19}Si(17)$  and  $C_{19}Si(20)$ . (E) In the Schlegel diagram, the blue dots represent the position of the heteroatoms that resulted in geometrical conformers with the characteristics shown in  $C_{19}Si(A)$ . The red dots indicate the positions of the heteroatoms that resulted in geometrical conformers with the characteristics shown in  $C_{19}Si(B)$ .

Our results confirm that the doping of  $C_{20}$  with a Si atom generates a structural and electronic variation that depends on the position in which the impurity is inserted into the fullerene cage. However, only two types of  $C_{19}Si$  geometrical conformations were retrieved. To simplify the discussion, these sets of substitutions will be referred to as the  $C_{19}Si(A)$  set and the  $C_{19}Si(B)$  set. Both sets are represented by Figure 2C,D, respectively.

The  $C_{19}Si(A)$  set contains the following doped fullerenes:  $C_{19}Si(1)$ ,  $C_{19}Si(2)$ ,  $C_{19}Si(4)$ ,  $C_{19}Si(6)$ ,  $C_{19}Si(7)$ ,  $C_{19}Si(8)$ ,  $C_{19}Si(11)$ ,  $C_{19}Si(12)$ ,  $C_{19}Si(13)$ ,  $C_{19}Si(14)$ ,  $C_{19}Si(15)$ ,  $C_{19}Si(16)$ ,  $C_{19}Si(17)$ ,  $C_{19}Si(18)$  and  $C_{19}Si(19)$ . The  $C_{19}Si(B)$  set is formed by the doped fullerenes  $C_{19}Si(3)$ ,  $C_{19}Si(5)$ ,  $C_{19}Si(9)$ ,  $C_{19}Si(10)$ ,  $C_{19}Si(17)$  and  $C_{19}Si(20)$ . Looking at Figure 2 and Table 1, the  $C_{19}Si(A)$  and  $C_{19}Si(B)$  sets have similar members with close structural similarity, and the same tendency of charge accumulation on the Si atom, the same values of  $E_{HL}$  in addition to the same total energy.

**Table 1.** MK charges on the Si-atom, total energy,  $E_t$ , (in a.u.) HOMO energy,  $E_H$ , LUMO energy,  $E_L$ , and HOMO-LUMO energy gap  $E_{HL}$ , (in eV) also shown for discussion in the text. The last column presents the relative population,  $\eta$  in %, of each of the geometrical conformers calculated using the Boltzmann distribution at 298.15 K.

	MK	$E_t$	$E_H$	$E_L$	$E_{HL}$	$\eta$
C <sub>19</sub> Si (1)	1.033	−1012.718	−7.237	−2.439	4.798	~0
C <sub>19</sub> Si (2)	1.044	−1012.718	−7.237	−2.439	4.798	~0
C <sub>19</sub> Si (3)	−0.174	−1012.777	−7.765	−2.047	5.718	16.784
C <sub>19</sub> Si (4)	1.033	−1012.718	−7.237	−2.439	4.798	~0
C <sub>19</sub> Si (5)	−0.173	−1012.777	−7.763	−2.047	5.716	16.590
C <sub>19</sub> Si (6)	1.044	−1012.718	−7.237	−2.438	4.799	~0
C <sub>19</sub> Si (7)	1.034	−1012.718	−7.237	−2.436	4.801	~0
C <sub>19</sub> Si (8)	1.034	−1012.718	−7.237	−2.436	4.801	~0
C <sub>19</sub> Si (9)	−0.185	−1012.777	−7.763	−2.048	5.716	16.555
C <sub>19</sub> Si (10)	−0.185	−1012.777	−7.763	−2.047	5.716	16.590
C <sub>19</sub> Si (11)	1.033	−1012.718	−7.237	−2.439	4.798	~0
C <sub>19</sub> Si (12)	1.033	−1012.718	−7.237	−2.447	4.790	~0
C <sub>19</sub> Si (13)	1.045	−1012.718	−7.237	−2.436	4.801	~0
C <sub>19</sub> Si (14)	1.044	−1012.718	−7.237	−2.439	4.798	~0
C <sub>19</sub> Si (15)	1.045	−1012.718	−7.237	−2.436	4.801	~0
C <sub>19</sub> Si (16)	1.033	−1012.718	−7.237	−2.447	4.790	~0
C <sub>19</sub> Si (17)	−0.178	−1012.777	−7.765	−2.047	5.718	16.784
C <sub>19</sub> Si (18)	1.044	−1012.718	−7.237	−2.439	4.798	~0
C <sub>19</sub> Si (19)	1.044	−1012.718	−7.237	−2.439	4.798	~0
C <sub>19</sub> Si (20)	−0.162	−1012.777	−7.765	−2.044	5.722	16.696

Thus, it can be seen in Table 1, that the  $E_{HL}$  energy also presents different values depending on the position of the heteroatom. If the heteroatom is positioned to generate geometrical conformations of the C<sub>19</sub>Si (B) set (Figure 2D),  $E_{HL}$  tends to increase. On the other hand, if the heteroatom replaces one of the carbons as indicated in C<sub>19</sub>Si (A) (Figure 2C),  $E_{HL}$  tends to decrease. Considering that the variation of  $E_{HL}$  is an indication of chemical stability in which higher values of  $E_{HL}$  indicate a reduction in the chemical reactivity of a given molecule [66], we note from Table 1, that the geometrical conformers pertaining to C<sub>19</sub>Si (B) set are more chemically stable than those of the C<sub>19</sub>Si (A) set. Relying on B3LYP/3-21G calculations, Ajeel and coworker [29] did not observe significant changes in the  $E_{HL}$  energy and in the structural properties of C<sub>19</sub>Si. Since only three out of ten C<sub>19</sub>Si geometrical conformers belong to the C<sub>19</sub>Si (B) set, a non-rational choice of doping site increases the odds of producing a C<sub>19</sub>Si (A) geometrical conformer.

Again, in Table 1, total electronic energy  $E_t$  of the molecules was also considered to understand their relative stability. For the geometrical conformers of the C<sub>19</sub>Si (A) set  $E_t = -1012.718$  a.u., whereas for the C<sub>19</sub>Si (B) set  $E_t = -1012.777$  a.u. Thus, based on this total energy criteria, the geometrical conformers of the C<sub>19</sub>Si (B) set are more stable than those of the C<sub>19</sub>Si (A) set corroborating the conclusions on the chemical stability made by comparing the values of  $E_{HL}$ .

Table 1 also brings the relative population,  $\eta$ , of geometrical conformers based on a Boltzmann distribution, at 298.15 K, revealing that the molecules of the C<sub>19</sub>Si (A) group are close to zero while those of C<sub>19</sub>Si (B) are vastly dominant. We expect therefore, that geometrical conformers belonging to the C<sub>19</sub>Si (B) will be more likely produced in a synthesis of C<sub>19</sub>Si. Based on these calculations, it is observed that, in theory, the doping site can be chosen to generate the desired structural and electronic properties for each application. Consequently, the C<sub>19</sub>Si (10) was selected to be studied as a promising molecule to interact with the gas molecules, because C<sub>19</sub>Si (10) showed to be the most stable geometrical conformer belonging to the C<sub>19</sub>Si (B).

### 3.2. Adsorption Energies between $C_{20}$ Fullerene and CO, $CO_2$ and $N_2$ Molecules

Now let's turn our attention to the interacting energies between the investigated chemical species. Table S2 presents the respective coordinates of the dimers formed between the  $C_{20}$  and  $C_{19}Si$  fullerenes and the CO,  $CO_2$  and  $N_2$  molecules. In its pristine form, CO,  $CO_2$  and  $N_2$  molecules are adsorbed in a parallel orientation as shown in the molecular representations of the dimers in Table S7. The BSSE-corrected adsorption energy,  $E_{ads}$ , obtained through Equation (1), portrayed in Figure 3 and in Table S5.

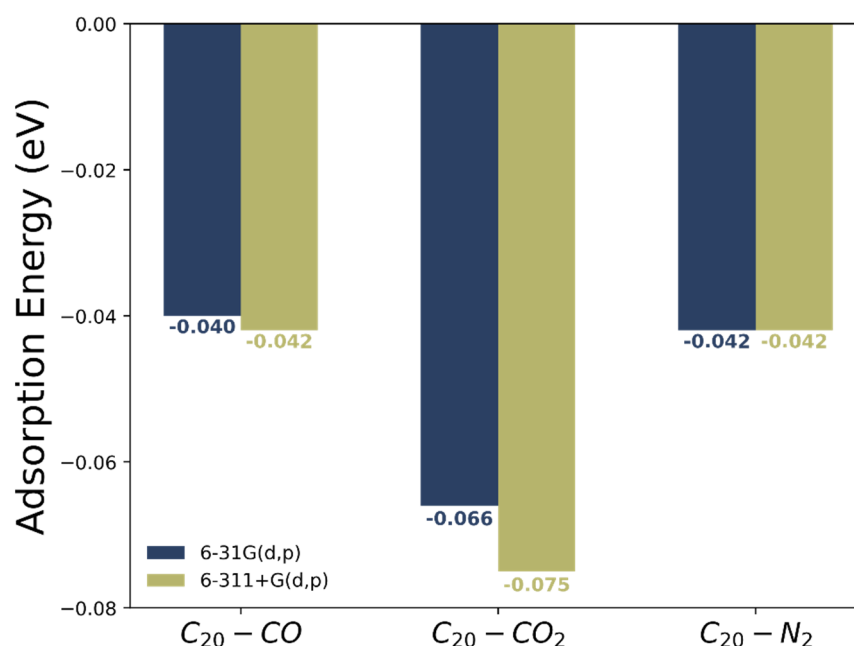


**Figure 3.** Adsorption energies (in eV),  $E_{ads}$ , for the dimers formed between  $C_{20}$  fullerenes with CO,  $CO_2$  and  $N_2$  molecules calculated with the theoretical levels  $\omega B97XD/6-31G(d)$  and  $\omega B97XD/6-311+G(d,p)$ .

From Figure 3 we note that both theoretical models point to the  $C_{20}-CO_2$  as the most interacting structure with highest value of  $E_{ads}$  among the analyzed dimers. Interaction energies of  $C_{20}-CO$  and  $C_{20}-N_2$  are dissimilar, so there is no clear selectivity towards these two molecules. Our theoretical results indicate that the complexes studied in the present work are about twice as stable as the complexes investigated by Vessally et al. [33], which can be attributed to both the basis set and the functional chosen for the calculation.

To verify the sensitivity of  $C_{20}$  in relation to the adsorption of CO,  $CO_2$  and  $N_2$  molecules, the energy gap,  $E_{HL}$ , of the dimers formed after the adsorption of the gases, was compared with its value prior to the adsorption of the gases. The results of this comparison are presented as a percentual change, represented by  $\Delta E_{HL}$ . The results of  $\Delta E_{HL}$  can be seen in Table S7. In general, it is observed that the HOMO-LUMO gap is nearly insensitive to the presence of the interacting gases with  $\Delta E_{HL} \sim 0$  in the absence of any EOEF. Thus,  $C_{20}$  fullerene is not sensitive for the detection of CO,  $CO_2$  and  $N_2$  molecules.

### 3.3. Electric Field Effect on the Adsorption Energies

To investigate the influence of the electric field, in both structural and energetic characteristics, adsorption calculations for the doped systems were performed. Following we report our findings following the increase of  $F$ .

$$F = 0.000 \text{ a.u.} \quad (2)$$

The results indicate that the adsorption energies, when compared to the  $E_{ads}$  values of the dimers formed with the gases and the pristine fullerenes, increased for the adsorption

of carbon monoxide and carbon dioxide. For  $C_{19}Si-N_2$ , a decrease in the energy module  $E_{ads}$  is observed when the calculation is performed with the level  $\omega B97XD/6-31G(d)$ .

For ease of interpretation, the energy values for the second theoretical level are shown in parentheses. The results show that  $E_{ads}$  increases to  $-0.703$  eV ( $-0.738$  eV) for  $C_{19}Si-CO$  and  $-0.068$  eV ( $-0.077$  eV) for  $C_{19}Si-CO_2$ .  $E_{ads}$  obtained with  $\omega B97XD/6-311+G(d,p)$ , resulted in a slight increase in the interaction between nitrogen gas and doped fullerene ( $E_{ads}$  values observed for the  $C_{19}Si-N_2$  dimer were  $-0.017$  eV ( $-0.045$  eV)). As can be seen in the Figures in Table S10 for  $C_{19}Si-CO$ , the CO reorients to interact in a perpendicular configuration. For  $C_{19}Si-CO_2$  and  $C_{19}Si-N_2$ , the molecules remain interacting in a parallel orientation.

Since the CO molecule has a permanent dipole moment, in which the carbon atom has a positive charge and the oxygen atom has a negative charge, the interaction between the CO molecule and  $C_{19}Si$  is expected to be the most favorable among the three chemicals analyzed. This is most likely due to the nucleophilic behavior observed on the Si atom in  $C_{19}Si$  fullerene. This charge accumulation on the heteroatom favors the adsorption of CO in the doped cage through a directional dipolar interaction. The results for the doped system are detailed in Table S6 and in the Figures in Table S10.

The percentage variation of the energy gap between the frontier orbitals,  $\Delta E_{HL}$ , indicates that  $C_{19}Si$  is highly sensitive to the detection of carbon monoxide, and, as can be seen in Table S7,  $\Delta E_{HL} \sim 20\%$  for the two theoretical levels. The negative sign indicates a reduction in the energy gap. For  $CO_2$  and  $N_2$ ,  $\Delta E_{HL}$  values show no significant changes, i.e.,  $C_{19}Si$  is not sensitive to the presence of  $CO_2$  and  $N_2$ .

$$F \neq 0.000 \text{ a.u.} \quad (3)$$

As can be seen in Tables S6 and S10 and in Figure 4, for both calculation levels, the  $E_{ads}$  values for  $F = 0.001$  a.u. are very similar to the  $E_{ads}$  values in the absence of the electric field. From the Figures in Table S10, it is noted that the effects of the electric field,  $F = 0.001$  a.u., is to reorient the  $CO_2$  and  $N_2$  molecules, so that they interact with a pentagonal face of the  $C_{19}Si$  cage, which has a more electrophilic character (see Figure 1E). Table S7 shows that as the electric field increases in intensity, the energy gap reduces correspondingly for all dimers, and this effect is more pronounced when  $C_{19}Si$  absorbs  $CO_2$  and  $N_2$ . The  $\omega B97XD/6-311+G(d,p)$  derived  $\Delta E_{HL}$  values, with the strongest electric field  $F = 0.025$  a.u., of the  $C_{19}Si-CO_2$  and  $C_{19}Si-N_2$  dimers is very close to the variation observed for the  $C_{19}Si-CO$  dimer. However, even for this strong  $F$ ,  $C_{19}Si$  presents greater sensitivity for the detection of the CO molecule.

Now let's discuss the EOEf effect on the adsorption energies for the doped fullerene with  $F$  the range of  $0.005$  a.u. and  $0.025$  a.u., presented in Figure 4. We note from Table S6 and Figure 4 that  $F$  and  $E_{ads}$  show direct proportionality, and for the  $C_{19}Si-CO$  system, this increase appears almost linear. On the other hand, for the  $C_{19}Si-CO_2$  and  $C_{19}Si-N_2$  systems,  $F$  affects  $E_{ads}$ , with a prominent parabolic behavior as corroborated by fitting correlation polynomial expressions on the  $F$  vs.  $E_{ads}$  portrayed in Figure 4. Clearly, such correlation equations are valid only within the range of  $F$  considered in this work, so that even further increasing in the electric field tends to decrease the separation of the molecules and eventually steric repulsions start to dominate.

### 3.4. Intermolecular Interaction Characterization under EOEf Influence

To investigate the character of the intermolecular interactions, we employed QTAIM and RDG analyses. QTAIM analysis allows for investigation of the nature of intra/intermolecular interactions relying on topological properties of the electron density. The use of QTAIM analysis has been successful in characterizing and describing interactions in various chemical systems [60,61,67–70].

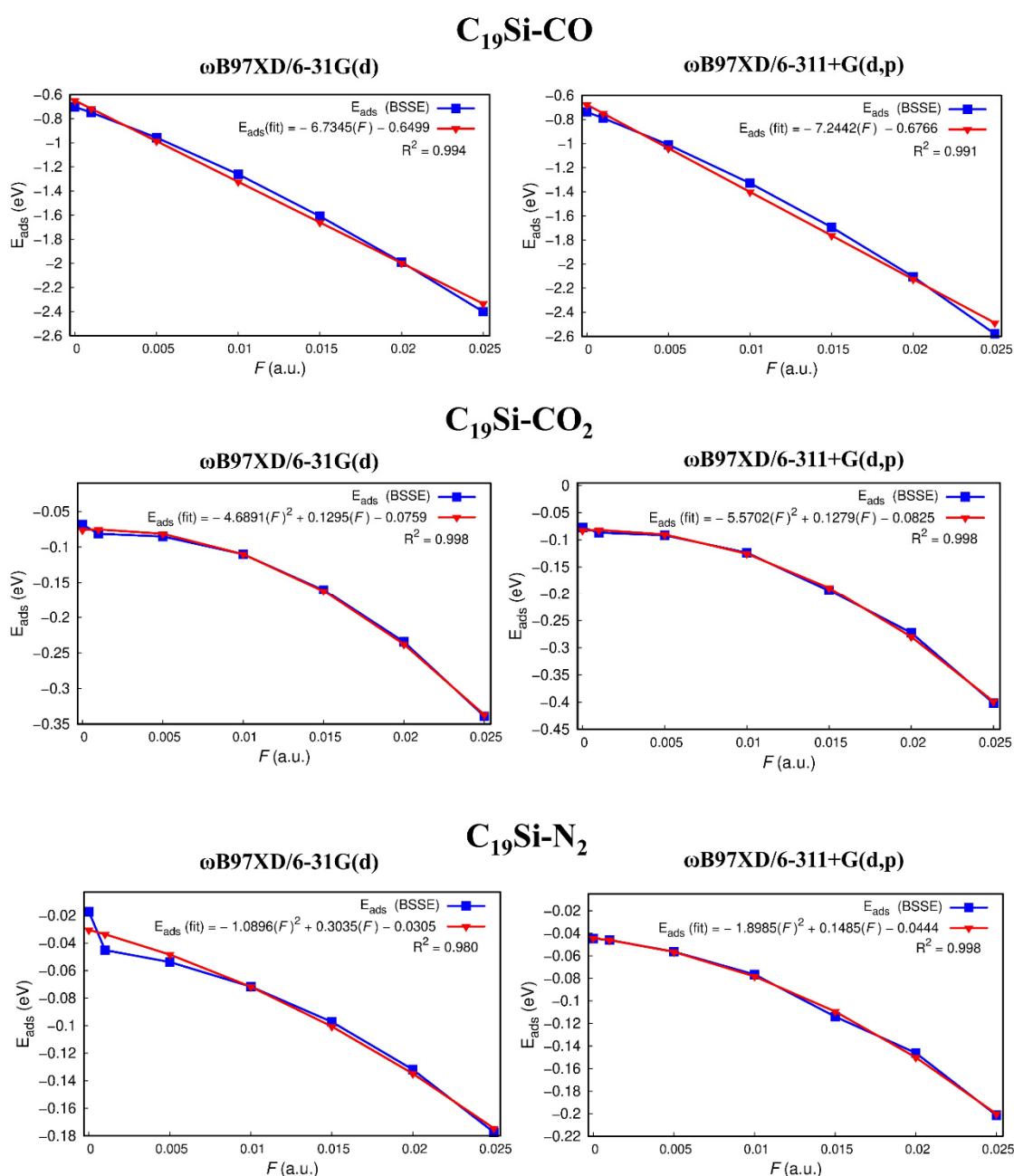


**Figure 4.** Theoretical,  $E_{\text{ads}}$ , and fitted,  $E_{\text{ads}}(\text{fit})$ , adsorption energies as a function of the electric field,  $F$ .

The results obtained for the pure and doped dimers are shown in Tables S8–S10. It is observed that, for all dimers in pure form, with  $F = 0$ , the values of the electron density,  $\rho_{\text{BCP}}$ , are in the order of  $10^{-3}e/a_0^3$ . The Laplacian values of electron density,  $\nabla\rho_{\text{BCP}}^2$ , always have positive values. Furthermore, the ratio of kinetic energy density to potential energy density,  $|G_{\text{BCP}}/V_{\text{BCP}}|$  have values greater than one unit. These results of  $\rho_{\text{BCP}}$ ,  $\nabla\rho_{\text{BCP}}^2$  and  $|G_{\text{BCP}}/V_{\text{BCP}}|$  indicate that  $\text{C}_{20}\text{-CO}$ ,  $\text{C}_{20}\text{-CO}_2$  and  $\text{C}_{20}\text{-N}_2$  dimers are stabilized primarily through van der Waals (vdW) interactions. The RDG scatter plot and the isosurfaces presented in the Figures in Table S10 corroborate these observations.

For doped fullerenes, as can be seen in Tables S8–S10, the dimers  $\text{C}_{19}\text{Si-CO}_2$  and  $\text{C}_{19}\text{Si-N}_2$  continue to present values of  $\rho_{\text{BCP}}$ ,  $\nabla\rho_{\text{BCP}}^2$  and  $|G_{\text{BCP}}/V_{\text{BCP}}|$  consistent with observed values for vdW interactions [71–78]. These results remain for the two theoretical levels and for  $F < 0.025 \text{ a.u.}$  The RDG scatter plots, for both calculation levels, confirm the non-covalent character of vdW-type observed by the QTAIM analyses. When  $F = 0.025 \text{ a.u.}$ ,

the QTAIM parameters and the RDG plot indicate that the interaction changes from vdW to a dipolar character for C<sub>19</sub>Si-CO<sub>2</sub>. When C<sub>19</sub>Si-N<sub>2</sub> is considered, the interaction between the N<sub>2</sub> atom and the doped is still of vdW-type.

For the C<sub>19</sub>Si-CO dimer, the results for the two theoretical levels indicate higher values of  $\rho_{BCP}$ , (about  $10^{-2}e/a_0^3$ ), for all values electric field. The values of  $\nabla\rho_{BCP}^2$  remain positive and  $|G_{BCP}/V_{BCP}| < 1$ . According to the characterization of the QTAIM parameters [71–78], C<sub>19</sub>Si-CO shows a dipolar interaction character, at the  $\omega$ B97XD/6-31G(d) level and a polar-covalent character for the  $\omega$ B97XD/6-311+G(d,p) level when  $F < 0.0150$  a.u.. Beyond  $F = 0.015$  a.u., C<sub>19</sub>Si starts to show a tendency to interact with CO through an interaction with partial polar-covalent character for both theoretical levels. This observation agrees with the characteristics observed in the MEP of C<sub>19</sub>Si (Figure 1), with the  $E_{ads}$  values obtained for C<sub>19</sub>Si-CO (Table S6) and with the directionality observed for the interaction between CO and C<sub>19</sub>Si shown in Table S10.

An interesting fact was observed in the analysis of QTAIM in the C<sub>19</sub>Si-CO system with the theoretical level  $\omega$ B97XD/6-31G(d). For this complex, the presence of critical degenerate points was observed in the intermolecular region between the Si and O atoms, as can be seen in Table S10. This type of degeneracy is common in stability studies, especially in structures under the influence of an external factor such as temperature or in solvents [79–82]. Degenerate critical points are usually associated with unstable interactions [83]. The closer the RCP and the BCP are, the more unstable the interaction tends to be. In unstable interactions, a small energy disturbance can cause migration from an RCP to a BCP, which leads to the disappearance of RCP [83]. However, when the basis set was extended, this degeneracy disappears.

#### 4. Conclusions

With the interest of investigating the adsorption of carbon monoxide, CO, carbon dioxide, CO<sub>2</sub>, and nitrogen gas, N<sub>2</sub>, the C<sub>20</sub> fullerene was Si-doped. To investigate the impact of heteroatom positioning in the C<sub>20</sub> cage, twenty C<sub>19</sub>Si were produced. In the present investigation, the Si substitution position influenced the structural and electronic characteristics of the doped system. This led to the formation of two groups of geometrical conformers, namely C<sub>19</sub>Si (A) and C<sub>19</sub>Si (B), classified according to their deformations. After an energetic analysis, it was observed that only the geometrical conformer of the C<sub>19</sub>Si(B) group are energetically favorable at the temperature of 298.15 K.

The adsorption of CO, CO<sub>2</sub> and N<sub>2</sub> was not favorable to the C<sub>20</sub> fullerene cage from the energetic point of view. However, it can be observed that the doping with a Si atom enabled the adsorption of the chemical species mentioned to the C<sub>19</sub>Si cage. This adsorption was intensified for all molecules aided by an externally oriented electric field. However, the formation of the C<sub>19</sub>Si-CO dimer was the most favored. Thus, C<sub>19</sub>Si has good selectivity in the adsorption of CO over CO<sub>2</sub> and N<sub>2</sub>. Based on energetic and topological parameters, when the intensity of the EOEF is smaller than  $F < 0.015$  a.u., physisorption take place between CO and C<sub>19</sub>Si. Further increasing  $F$ , the adsorption shifts to a polar-covalent character as revealed by QTAIM parameters.

Adsorption energies shows a quadratic relationship with the EOEF with C<sub>19</sub>Si-CO<sub>2</sub> and C<sub>19</sub>Si-N<sub>2</sub> dimers, and a linear dependence in the case of C<sub>19</sub>Si-CO. Obtaining the correlations for the interaction of these molecules with C<sub>19</sub>Si enable the ration use of EOEF to capture gaseous chemical species. DFT calculations revealed that C<sub>19</sub>Si fullerene is good prototype to selectively detection of carbon monoxide. Modulating the intensity of the EOEF C<sub>19</sub>Si displays is suitable for a CO uptake and detection.

**Supplementary Materials:** The following supporting information can be downloaded at: <https://www.mdpi.com/article/10.3390/molecules27092968/s1>, Figure S1: Orientation of the electric field vector with respect to the C<sub>19</sub>Si cage; Table S1: Optimized coordinates for C<sub>20</sub> and C<sub>19</sub>Si fullerenes at theoretical levels  $\omega$ B97XD/6-31G(d) and  $\omega$ B97XD/6-311+G(d,p). Electric field  $F$  in atomic units and Total energies in hartree; Table S2: Optimized coordinates for the dimers formed by pure and doped fullerenes and CO, CO<sub>2</sub> and N<sub>2</sub> gases in each of the studied field values. Electric field  $F$  in atomic units

and BSSE-corrected adsorption energies in electron-volts; Table S3: Frontier orbital energies (in eV) for C<sub>20</sub> and C<sub>19</sub>Si fullerenes. Percentual increase of the HOMO-LUMO gap,  $\Delta E_{HL}$  is also shown; Table S4: Si-C bond lengths and Merz-Kollmann (MK) charges on the Si-atom and adjacent carbons.; Table S5: Adsorption energies (in eV),  $E_{ads}$ , and adsorption energy with and without BSSE corrections,  $E_{ads}$  (BSSE), for the dimers formed between C<sub>20</sub> fullerenes with CO, CO<sub>2</sub> and N<sub>2</sub> molecules calculated with the theoretical levels  $\omega$ B97XD/6-31G(d) and  $\omega$ B97XD/6-311+G(d,p); Table S6: Externally oriented electric field effect on the BSSE correction, adsorption energies,  $E_{ads}$ , and BSSE corrected,  $E_{ads}$  (BSSE), for the interaction of C<sub>20</sub> and C<sub>19</sub>Si fullerenes with the CO, CO<sub>2</sub> and N<sub>2</sub> molecules as obtained at the  $\omega$ B97XD/6-31G(d) and  $\omega$ B97XD/6-311+G(d,p) levels of theory. Adjusted adsorption energy,  $E_{ads}$  (fit) and the R-squared coefficient of determination, R<sup>2</sup>, are also presented. All energies in eV; Table S7: Topological parameters calculated using the Quantum Theory of Atoms in Molecules (QTAIM) with the theoretical level  $\omega$ B97XD/6-31G(d). Results are presented for all dimers formed by C<sub>20</sub> and C<sub>19</sub>Si fullerenes with adsorbed gas molecules. The results were obtained for all electric field values and are all presented in atomic units; Table S8: Topological parameters calculated using the Quantum Theory of Atoms in Molecules (QTAIM) with the theoretical level  $\omega$ B97XD /6-311+G(d,p). Results are presented for all dimers formed by C<sub>20</sub> and C<sub>19</sub>Si fullerenes with adsorbed gas molecules. The results were obtained for all electric field values and are all presented in atomic units; Table S9: Critical bond points, BCP, isosurfaces and scatter plots for the dimers formed by C<sub>20</sub> and C<sub>19</sub>Si fullerenes with the adsorbed gas molecules. The results were obtained for all electric field values using both the theoretical level  $\omega$ B97XD/6-31G(d) and  $\omega$ B97XD/6-311+G(d,p); Table S10: Energies (in eV) of the HOMO, E<sub>H</sub>, LUMO, E<sub>L</sub> and the gap between them, E<sub>HL</sub>, calculated with the theoretical levels  $\omega$ B97XD/6-31G(d) and  $\omega$ B97XD/6-311+G(d,p), for the dimers. The percentual change in the fullerene energy gap after adsorbing the gas, in relation to the fullerene energy gap before adsorption, is represented by  $\Delta E_{HL}$  (in %). Positive values of  $\Delta E_{HL}$  indicate an increase in the gap, negative values indicate a reduction.

**Author Contributions:** R.A.L.S. and D.F.S.M. designed the project, R.A.L.S., D.F.S.M. and H.C.B.d.O. performed the data analysis. R.A.L.S. wrote original draft preparation, R.A.L.S., N.M.N.R., D.A.d.S.F., H.C.B.d.O. and L.R writing—review and editing. R.A.L.S., D.A.d.S.F. and L.R. carried out the calculations. All authors have read and agreed to the published version of the manuscript.

**Funding:** This research was funded in part by the Coordenação de Aperfeiçoamento de Pessoal de Nível Superior—Brasil (CAPES)—Finance Code 001 (Convênio n° 817164/2015 CAPES/PROAP), and by Conselho Nacional de Desenvolvimento Científico e Tecnológico (CNPq-grants 164561/2017-0) and Coordenação de Aperfeiçoamento Pessoal de Nível Superior (CAPES), and Fundação de Apoio à Pesquisa do Distrito Federal (FAP-DF), and Fundação de Amparo à Pesquisa do Estado de Goiás (FAPEG). D.A.S.F. acknowledges the financial support from the Edital DPI-UnB No. 02/2021, from CNPq (grants 305975/2019-6, and 420836/2018-7) and FAP-DF (grants 193.001.596/2017 and 193-00001220/2021-37).

**Institutional Review Board Statement:** Not applicable.

**Informed Consent Statement:** Not applicable.

**Data Availability Statement:** The data presented in this study are available in the article and in the Supplementary Material.

**Conflicts of Interest:** The authors declare no conflict of interest. The funders had no role in the design of the study; in the collection, analyses, or interpretation of data; in the writing of the manuscript, or in the decision to publish the results.

## References

1. Yang, C.M.; Chen, T.C.; Yang, Y.C.; Hsiao, M.C.; Meyyappan, M.; Lai, C.S. Ultraviolet illumination effect on monolayer graphene-based resistive sensor for acetone detection. *Vacuum* **2017**, *140*, 89–95. [[CrossRef](#)]
2. Nomani, M.W.K.; Shishir, R.; Qazi, M.; Diwan, D.; Shields, V.B.; Spencer, M.G.; Tompa, G.S.; Sbrockey, N.M.; Koley, G. Highly sensitive and selective detection of NO<sub>2</sub> using epitaxial graphene on 6H-SiC. *Sens. Actuators B Chem.* **2010**, *150*, 301–307. [[CrossRef](#)]
3. Romero, H.E.; Joshi, P.; Gupta, A.K.; Gutierrez, H.R.; Cole, M.W.; Tadigadapa, S.A.; Eklund, P.C. Adsorption of ammonia on graphene. *Nanotechnology* **2009**, *20*, 245501. [[CrossRef](#)] [[PubMed](#)]

4. Justino, C.I.L.; Gomes, A.R.; Freitas, A.C.; Duarte, A.C.; Rocha-Santos, T.A.P. Graphene based sensors and biosensors. *TrAC Trends Anal. Chem.* **2017**, *91*, 53–66. [[CrossRef](#)]
5. Feng, X.; Zhang, Y.; Zhou, J.; Li, Y.; Chen, S.; Zhang, L.; Ma, Y.; Wang, L.; Yan, X. Three-dimensional nitrogen-doped graphene as an ultrasensitive electrochemical sensor for the detection of dopamine. *Nanoscale* **2015**, *7*, 2427–2432. [[CrossRef](#)]
6. Li, X.; Zhao, H.; Shi, L.; Zhu, X.; Lan, M.; Zhang, Q.; Hugh Fan, Z. Electrochemical sensing of nicotine using screen-printed carbon electrodes modified with nitrogen-doped graphene sheets. *J. Electroanal. Chem.* **2017**, *784*, 77–84. [[CrossRef](#)]
7. Kroto, H.W.; Walton, D.R.M. Stable derivatives of small fullerenes. *Chem. Phys. Lett.* **1993**, *214*, 353–356. [[CrossRef](#)]
8. Osawa, E.; Kroto, H.W.; Fowler, P.W.; Wasserman, E. The evolution of the football structure for the C<sub>60</sub> molecule: A retrospective. *Philos. Trans. R. Soc. A Math. Phys. Eng. Sci.* **1993**, *343*, 1–8. [[CrossRef](#)]
9. Kroto, H.W. The stability of the fullerenes C<sub>n</sub>, with n = 24, 28, 32, 36, 50, 60 and 70. *Nature* **1987**, *329*, 529–531. [[CrossRef](#)]
10. Mojica, M.; Alonso, J.A.; Méndez, F. Synthesis of fullerenes. *J. Phys. Org. Chem.* **2013**, *26*, 526–539. [[CrossRef](#)]
11. Silva, R.A.L.; de Brito, S.F.; Machado, D.F.S.; Carvalho-Silva, V.H.; de Oliveira, H.C.B.; Ribeiro, L. The influence of the configuration of the (C<sub>70</sub>)<sub>2</sub> dimer on its rovibrational spectroscopic properties: A theoretical survey. *J. Mol. Model.* **2018**, *24*, 235. [[CrossRef](#)] [[PubMed](#)]
12. MahdaviFar, Z.; Nomresaz, Z.; Shakerzadeh, E. Hetero-fullerenes C<sub>59</sub>M (M = B, Al, Ga, Ge, N, P, As) for sulfur dioxide gas sensing: Computational approach. *Chem. Phys.* **2020**, *530*, 110606. [[CrossRef](#)]
13. Heidari, M.; Janjanpour, N.; Vakili, M.; Daneshmehr, S.; Jalalierad, K.; Alipour, F. Study of the Ionization Potential, Electron Affinity and HOMO-LUMO Gaps in the Small Fullerene Nanostructures. *Chem. Rev. Lett.* **2018**, *1*, 45–48.
14. Motlagh, N.M.; Rouhani, M.; Mirjafary, Z. Aminated C<sub>20</sub> fullerene as a promising nanosensor for detection of A-234 nerve agent. *Comput. Theor. Chem.* **2020**, *1186*, 112907. [[CrossRef](#)]
15. Metin, T.; Parlak, C.; Alver, Ö.; Tepe, M. Hydrogen storage and electronic properties of C<sub>20</sub>, C<sub>15</sub>M<sub>5</sub> and H<sub>2</sub>@C<sub>15</sub>M<sub>5</sub> (M = Al, Si, Ga, Ge) nanoclusters. *J. Mol. Struct.* **2021**, *1247*, 131272. [[CrossRef](#)]
16. Khan, A.A.; Ahmad, I.; Ahmad, R. Influence of electric field on CO<sub>2</sub> removal by P-doped C<sub>60</sub>-fullerene: A DFT study. *Chem. Phys. Lett.* **2020**, *742*, 137155. [[CrossRef](#)]
17. Stankevich, I.V.; Nikerov, M.V.; Bochvar, D.A. The Structural Chemistry of Crystalline Carbon: Geometry, Stability, and Electronic Spectrum. *Russ. Chem. Rev.* **1984**, *53*, 640–655. [[CrossRef](#)]
18. Prinzbach, H.; Weller, A.; Landenberger, P.; Wahl, F.; Wörth, J.; Scott, L.T.; Gelmont, M.; Olevano, D.; Issendorff, B.V. Gas-phase production and photoelectron spectroscopy of the smallest fullerene, C<sub>20</sub>. *Nature* **2000**, *407*, 60–63. [[CrossRef](#)]
19. Guo, B.C.; Kerns, K.P.; Castleman, A.W. Ti<sub>8</sub>C<sup>12+</sup>-metallo-carbohedrenes: A new class of molecular clusters? *Science* **1992**, *255*, 1411–1413. [[CrossRef](#)]
20. Slanina, Z.; Adamowicz, L. MNDO study of charged complexes of dodecahedron-shaped C<sub>20</sub> with Li. *J. Mol. Struct. THEOCHEM* **1993**, *281*, 33–37. [[CrossRef](#)]
21. Magoulas, K.; Tassios, D. Thermophysical properties of n-Alkanes from C<sub>1</sub> to C<sub>20</sub> and their prediction for higher ones. *Fluid Phase Equilib.* **1990**, *56*, 119–140. [[CrossRef](#)]
22. Deng, H.T.; Guo, B.C.; Kerns, K.P.; Castleman, A.W. Formation and stability of metallocarbohedrenes: Ti<sub>x</sub>M<sub>y</sub>C<sub>12</sub> (x + y = 8, M = Nb, Ta, Y, and Si). *Int. J. Mass Spectrom. Ion Process.* **1994**, *138*, 275–281. [[CrossRef](#)]
23. Hassanpour, A.; Nezhad, P.D.K.; Hosseinian, A.; Ebadi, A.; Ahmadi, S.; Ebrahimiasl, S. Characterization of IR spectroscopy, APT charge, ESP maps, and AIM analysis of C<sub>20</sub> and its C<sub>20</sub>-nAl<sub>n</sub> heterofullerene analogous (n = 1–5) using DFT. *J. Phys. Org. Chem.* **2021**, *34*, e4198. [[CrossRef](#)]
24. Huda, M.N.; Ray, A.K. Evolution of SiC nanocluster from carbon fullerene: A density functional theoretic study. *Chem. Phys. Lett.* **2008**, *457*, 124–129. [[CrossRef](#)]
25. Salem, M.A.; Katin, K.P.; Kaya, S.; Kochaev, A.I.; Maslov, M.M. Interaction of dopants and functional groups adsorbed on the carbon fullerenes: Computational study. *Phys. E Low-Dimens. Syst. Nanostruct.* **2020**, *124*, 114319. [[CrossRef](#)]
26. Rad, A.S.; Aghaei, S.M.; Aali, E.; Peyravi, M. Study on the electronic structure of Cr- and Ni-doped fullerenes upon adsorption of adenine: A comprehensive DFT calculation. *Diam. Relat. Mater.* **2017**, *77*, 116–121. [[CrossRef](#)]
27. Bai, H.; Wu, Y.; Qiao, W.; Ji, Y. Theoretical investigations on the geometrical structures, energies, and electronic properties of the heterofullerenes made of the smallest fullerene. *Fuller. Nanotub. Carbon Nanostruct.* **2015**, *23*, 399–405. [[CrossRef](#)]
28. Koohi, M.; Soleimani Amiri, S.; Shariati, M. Silicon impacts on structure, stability and aromaticity of C<sub>20</sub>-nSi<sub>n</sub> heterofullerenes (n = 1–10): A density functional perspective. *J. Mol. Struct.* **2017**, *1127*, 522–531. [[CrossRef](#)]
29. Ajeel, F.N.; Mohammed, M.H.; Khudhair, A.M. Tuning the electronic properties of the fullerene C<sub>20</sub> cage via silicon impurities. *Russ. J. Phys. Chem. B* **2017**, *11*, 850–858. [[CrossRef](#)]
30. Alver, Ö.; Parlak, C.; Umar, Y.; Ramasami, P. DFT/QTAIM analysis of favipiravir adsorption on pristine and silicon doped C<sub>20</sub> fullerenes. *Main Group Met. Chem.* **2019**, *42*, 143–149. [[CrossRef](#)]
31. Rouhani, M. Theoretical investigation about the adsorption of the Sarin nerve agent on C<sub>20</sub> fullerene and its boron-doped derivative. *Dispos. Am.* **2018**, *15*, 39–46. [[CrossRef](#)]
32. Ahmadi, R.; Jalali Sarvestani, M.R. Adsorption of proline amino acid on the surface of fullerene (C<sub>20</sub>) and boron nitride cage (B<sub>12</sub>N<sub>12</sub>): A comprehensive DFT study. *Q. J. Iran. Chem. Commun.* **2019**, *7*, 344–351. [[CrossRef](#)]
33. Vessally, E.; Siadati, S.A.; Hosseinian, A.; Edjlali, L. Selective sensing of ozone and the chemically active gaseous species of the troposphere by using the C<sub>20</sub> fullerene and graphene segment. *Talanta* **2017**, *162*, 505–510. [[CrossRef](#)] [[PubMed](#)]

34. Carratu, M.; Chen, Q.; Cotti, G.; Hazucha, M.; Jantunen, M.; Lahmann, E.; Lauriola, P.; Mathieu-Nolf, M.; Pankow, D.; Penney, D. *Environmental Health Criteria 213 Carbon Monoxide*; World Health Organisation: Geneva, Switzerland, 1999; pp. 1–101.
35. Léonard, N.G.; Dhaoui, R.; Chantarojsiri, T.; Yang, J.Y. Electric Fields in Catalysis: From Enzymes to Molecular Catalysts. *ACS Catal.* **2021**, *11*, 10923–10932. [[CrossRef](#)]
36. Yu, S.; Vermeeren, P.; Hamlin, T.A.; Bickelhaupt, F.M. How Oriented External Electric Fields Modulate Reactivity. *Chem.—Eur. J.* **2021**, *27*, 5683–5693. [[CrossRef](#)]
37. Sun, K.-B.; Zhang, S.-H.; Ren, F.-D.; Hao, Y.-P.; Ba, S.H. Theoretical prediction of the trigger linkage, cage strain, and explosive sensitivity of CL-20 in the external electric fields. *J. Mol. Model.* **2021**, *27*, 85. [[CrossRef](#)]
38. Li, Y.; Chen, J.; Zhao, C. Influence of external electric field on the electronic structure and optical properties of pyrite. *RSC Adv.* **2017**, *7*, 56676–56681. [[CrossRef](#)]
39. Khan, A.A.; Ahmad, R.; Ahmad, I.; Su, X. Selective adsorption of CO<sub>2</sub> from gas mixture by P-decorated C<sub>24</sub>N<sub>24</sub> fullerene assisted by an electric field: A DFT approach. *J. Mol. Graph. Model.* **2021**, *103*, 107806. [[CrossRef](#)]
40. Esrafil, M.D. Electric field assisted activation of CO<sub>2</sub> over P-doped graphene: A DFT study. *J. Mol. Graph. Model.* **2019**, *90*, 192–198. [[CrossRef](#)]
41. Song, N.; Wang, Y.; Gao, H.; Jiang, W.; Zhang, J.; Xu, B.; Sun, Q.; Jia, Y. Electric field improved hydrogen storage of Ca-decorated monolayer MoS<sub>2</sub>. *Phys. Lett. Sect. A Gen. At. Solid State Phys.* **2015**, *379*, 815–819. [[CrossRef](#)]
42. Liu, H.; Lee, J.Y. Electric field effects on the adsorption of CO on a graphene nanodot and the healing mechanism of a vacancy in a graphene nanodot. *J. Phys. Chem. C* **2012**, *116*, 3034–3041. [[CrossRef](#)]
43. Sun, Q.; Zhou, J.; Wang, Q.; Jena, P. Electric field enhanced hydrogen storage on polarizable materials substrates. *ACS Natl. Meet. B. Abstr.* **2010**, *107*, 2801–2806.
44. Baggio, A.R.; Machado, D.F.S.; Carvalho-Silva, V.H.; Paterno, L.G.; de Oliveira, H.C.B.; Kummel, A.C.; Trogler, W.C.; Sanyal, B.; Eriksson, O.; Puglia, C.; et al. Rovibrational spectroscopic constants of the interaction between ammonia and metallophthalocyanines: A theoretical protocol for ammonia sensor design. *Phys. Chem. Chem. Phys.* **2017**, *19*, 10843–10853. [[CrossRef](#)]
45. Ader, M.; Thomazo, C.; Sansjofre, P.; Busigny, V.; Papineau, D.; Laffont, R.; Cartigny, P.; Halverson, G.P. Interpretation of the nitrogen isotopic composition of Precambrian sedimentary rocks: Assumptions and perspectives. *Chem. Geol.* **2016**, *429*, 93–110. [[CrossRef](#)]
46. Nibe, M.; Svanborg, M.; Lemos-silva, R.; Da, D.A.; Filho, S.; Jørgensen, B.; Albrektsen, O.; Kjelstrup-hansen, J. Work function difference of naphthyl end-capped oligothiophene in different crystal alignments studied by Kelvin probe force microscopy. *Org. Electron.* **2021**, *89*, 106060. [[CrossRef](#)]
47. Nemati-Kande, E.; Abbasi, M.; Doust Mohammadi, M. DFT, QTAIM and NBO Investigation of the Interaction of Rare Gases with Pristine and Decorated Boron Nitride Nanotube. *ChemistrySelect* **2018**, *3*, 9833–9840. [[CrossRef](#)]
48. Agheli, Z.; Pordel, M.; Beyramabadi, S.A. Synthesis, characterization, optical properties, computational characterizations, QTAIM analysis and cyclic voltammetry of new organic dyes for dye-sensitized solar cells. *J. Mol. Struct.* **2020**, *1202*, 127228. [[CrossRef](#)]
49. Acharya, C.K.; Turner, C.H. Effect of an electric field on the adsorption of metal clusters on boron-doped carbon surfaces. *J. Phys. Chem. C* **2007**, *111*, 14804–14812. [[CrossRef](#)]
50. Boys, S.; Bernardi, F. The calculation of small molecular interactions by the differences of separate total energies. *Some procedures with reduced errors.* *Mol. Phys.* **1970**, *19*, 553–566. [[CrossRef](#)]
51. Bader, R.F.W. A quantum theory of molecular structure and its applications. *Chem. Rev.* **1991**, *91*, 893–928. [[CrossRef](#)]
52. Oliveira, B.G.; Araújo, R.C.M.U.; Ramos, M.N. A topologia molecular QTAIM e a descrição mecânico-quântica de ligações de hidrogênio e ligações de di-hidrogênio. *Quim. Nova* **2010**, *33*, 1155–1162. [[CrossRef](#)]
53. Bader, R.F.W.; Essén, H. The characterization of atomic interactions. *J. Chem. Phys.* **1984**, *80*, 1943. [[CrossRef](#)]
54. Contreras-García, J.; Johnson, E.R.; Keinan, S.; Chaudret, R.; Piquemal, J.; Beratan, D.N.; Yang, W. NCIPLOT: A Program for Plotting Noncovalent Interaction Regions. *J. Chem. Theory Comput.* **2011**, *7*, 625–632. [[CrossRef](#)] [[PubMed](#)]
55. Johnson, E.R.; Keinan, S.; Mori-Sánchez, P.; Contreras-García, J.; Cohen, A.J.; Yang, W. Revealing noncovalent interactions. *J. Am. Chem. Soc.* **2010**, *132*, 6498–6506. [[CrossRef](#)] [[PubMed](#)]
56. Frisch, M.J.; Trucks, G.W.; Schlegel, H.B.; Scuseria, G.E.; Robb, M.A.; Cheeseman, J.R.; Scalmani, G.; Barone, V.; Petersson, G.A.; Nakatsuji, H.; et al. *Gaussian 16, Revision C.01*; Gaussian, Inc.: Wallingford, CT, USA, 2016.
57. Lu, T.; Chen, F. Multiwfn: A multifunctional wavefunction analyzer. *J. Comput. Chem.* **2012**, *33*, 580–592. [[CrossRef](#)]
58. Humphrey, W.; Dalke, A.; Schulten, K. VMD: Visual molecular dynamics. *J. Mol. Graph.* **1996**, *14*, 33–38. [[CrossRef](#)]
59. Javan, M.B.; Ganji, M.D. Theoretical investigation on the encapsulation of atomic hydrogen into heterofullerene nanocages. *Curr. Appl. Phys.* **2013**, *13*, 1525–1531. [[CrossRef](#)]
60. Shariatinia, Z.; Shahidi, S. A DFT study on the physical adsorption of cyclophosphamide derivatives on the surface of fullerene C<sub>60</sub> nanocage. *J. Mol. Graph. Model.* **2014**, *52*, 71–81. [[CrossRef](#)]
61. Silva, R.A.L.; da Silva Filho, D.A.; Moberg, M.E.; Pappenfus, T.M.; Janzen, D.E. Halogen Interactions in Halogenated Oxindoles: Crystallographic and Computational Investigations of Intermolecular Interactions. *Molecules* **2021**, *26*, 5487. [[CrossRef](#)]
62. Bai, H.; Ji, W.; Liu, X.; Wang, L.; Yuan, N.; Ji, Y. Doping the buckminsterfullerene by substitution: Density functional theory studies of C<sub>59</sub>X (X = B, N, Al, Si, P, Ga, Ge, and As). *J. Chem.* **2012**, *2013*, 571709. [[CrossRef](#)]
63. Simeon, T.M.; Yanov, I.; Leszczynski, J. Ab initio quantum chemical studies of fullerene molecules with substitutes C<sub>59</sub>X [X = Si, Ge, Sn], C<sub>59</sub>X<sup>-</sup> [X = B, Al, Ga, In], and C<sub>59</sub>X<sup>+</sup> [X = N, P, As, Sb]. *Int. J. Quantum Chem.* **2005**, *105*, 429–436. [[CrossRef](#)]

64. Paul, D.; Deb, J.; Bhattacharya, B.; Sarkar, U. Density functional theory study of pristine and transition metal doped fullerene. *AIP Conf. Proc.* **2017**, *1832*, 1–4. [[CrossRef](#)]
65. Dheivamalar, S.; Sugi, L. Density functional theory (DFT) investigations on doped fullerene with heteroatom substitution. *Spectrochim. Acta Part A Mol. Biomol. Spectrosc.* **2015**, *151*, 687–695. [[CrossRef](#)]
66. Aihara, J.I. Reduced HOMO-LUMO Gap as an Index of Kinetic Stability for Polycyclic Aromatic Hydrocarbons. *J. Phys. Chem. A* **1999**, *103*, 7487–7495. [[CrossRef](#)]
67. Etminan, N.; Yoosefian, M.; Raissi, H.; Hakimi, M. Solvent effects on the stability and the electronic properties of histidine/Pd-doped single-walled carbon nanotube biosensor. *J. Mol. Liq.* **2016**, *214*, 313–318. [[CrossRef](#)]
68. Behjatmanesh-Ardakani, R.; Pourroustaei-Ardakani, F.; Taghdiri, M.; Kotena, Z.M. DFT-B3LYP study of interactions between host biphenyl-1-aza-18-crown-6 ether derivatives and guest Cd<sup>2+</sup>: NBO, NEDA, and QTAIM analyses. *J. Mol. Model.* **2016**, *22*, 149. [[CrossRef](#)] [[PubMed](#)]
69. Saadat, K.; Tavakol, H. An exceptional functionalization of doped fullerene observed via theoretical studies on the interactions of sulfur-doped fullerenes with halogens and halides. *RSC Adv.* **2015**, *5*, 55227–55237. [[CrossRef](#)]
70. Tariq, S.; Khalid, M.; Raza, A.R.; Rubab, S.L.; de Alcântara Morais, S.F.; Khan, M.U.; Tahir, M.N.; Braga, A.A.C. Experimental and computational investigations of new indole derivatives: A combined spectroscopic, SC-XRD, DFT/TD-DFT and QTAIM analysis. *J. Mol. Struct.* **2020**, *1207*, 127803. [[CrossRef](#)]
71. Grabowski, S.J. What Is the Covalency of Hydrogen Bonding? *Chem. Rev.* **2011**, *111*, 2597–2625. [[CrossRef](#)]
72. Lipkowski, P.; Grabowski, S.J.; Robinson, T.L.; Leszczynski, J. Properties of the C–H···H Dihydrogen Bond: An ab Initio and Topological Analysis. *J. Phys. Chem. A* **2004**, *108*, 10865–10872. [[CrossRef](#)]
73. Bianchi, R.; Gervasio, G.; Marabello, D. Experimental electron density analysis of Mn<sub>2</sub>(CO)<sub>10</sub>: Metal-metal and metal-ligand bond characterization. *Inorg. Chem.* **2000**, *39*, 2360–2366. [[CrossRef](#)] [[PubMed](#)]
74. Kumar, P.S.V.; Raghavendra, V.; Subramanian, V. Bader’s Theory of Atoms in Molecules (AIM) and its Applications to Chemical Bonding. *J. Chem. Sci.* **2016**, *128*, 1527–1536. [[CrossRef](#)]
75. Matta, C.F. Hydrogen-hydrogen bonding: The non-electrostatic limit of closed-shell interaction between two hydro. In *Hydrogen Bonding—New Insights*; Grabowski, S., Ed.; Springer: Łódź, Poland, 2006; pp. 337–375. ISBN 1402048521.
76. Berryman, V.E.J.; Whalley, Z.J.; Shephard, J.J.; Ochiai, T.; Price, A.N.; Arnold, P.L.; Parsons, S.; Kaltsoyannis, N. Computational analysis of M–O covalency in M(OC<sub>6</sub>H<sub>5</sub>)<sub>4</sub> (M = Ti, Zr, Hf, Ce, Th, U). *Dalt. Trans.* **2019**, *48*, 2939–2947. [[CrossRef](#)] [[PubMed](#)]
77. Ziolkowski, M.; Grabowski, S.J.; Leszczynski, J. Cooperativity in hydrogen-bonded interactions: Ab initio and “atoms in molecules” analyses. *J. Phys. Chem. A* **2006**, *110*, 6514–6521. [[CrossRef](#)] [[PubMed](#)]
78. Berryman, V.E.J.; Shephard, J.J.; Ochiai, T.; Price, A.N.; Arnold, P.L.; Parsons, S.; Kaltsoyannis, N. Quantum chemical topology and natural bond orbital analysis of M–O covalency in M(OC<sub>6</sub>H<sub>5</sub>)<sub>4</sub> (M = Ti, Zr, Hf, Ce, Th, Pa, U, Np). *Phys. Chem. Chem. Phys.* **2020**, *22*, 16804–16812. [[CrossRef](#)] [[PubMed](#)]
79. Astakhov, A.V.; Chernyshev, V.M. Molecular structure of 3-amino[1,2,4]triazolo-[4,3-a]pyrimidin-5-one in various tautomeric forms: Investigation by DFT and Qtaim methods. *Chem. Heterocycl. Compd.* **2014**, *50*, 319–326. [[CrossRef](#)]
80. Baryshnikov, G.V.; Minaev, B.F.; Minaeva, V.A.; Baryshnikova, A.T. Structure and intramolecular stabilization of geometric isomers of Bi- and trithiazolidine-4-ones and their methyl derivatives: A DFT and QTAIM study. *J. Struct. Chem.* **2012**, *53*, 428–435. [[CrossRef](#)]
81. Baryshnikov, G.V.; Minaev, B.F.; Korop, A.A.; Minaeva, V.A.; Gusev, A.N. Structure of zinc complexes with 3-(pyridin-2-yl)-5-(arylideneiminophenyl)-1H-1,2,4-triazoles in different tautomeric forms: DFT and QTAIM study. *Russ. J. Inorg. Chem.* **2013**, *58*, 928–934. [[CrossRef](#)]
82. Ayarde-Henríquez, L.; Guerra, C.; Duque-Noreña, M.; Rincón, E.; Pérez, P.; Chamorro, E. Are There Only Fold Catastrophes in the Diels-Alder Reaction between Ethylene and 1,3-Butadiene? *J. Phys. Chem. A* **2021**, *125*, 5152–5165. [[CrossRef](#)]
83. Bader, R.F.W. *Atoms in Molecules: A Quantum Theory*; Clarendon Press: Oxford, UK, 1990; ISBN 9780198558651.